Review of Scientific Instruments

Improving the electrostatic design of the Jefferson Lab 300 kV DC photogun

Cite as: Rev. Sci. Instrum. **93**, 073303 (2022); https://doi.org/10.1063/5.0091134
Submitted: 11 March 2022 • Accepted: 23 May 2022 • Published Online: 11 July 2022

S. A. K. Wijethunga, M. A. Mamun, R. Suleiman, et al.

Review of Scientific Instruments | ARTICLE | scitation.org/journal/rsi

Improving the electrostatic design of the Jefferson Lab 300 kV DC photogun

Cite as: Rev. Sci. Instrum. 93, 073303 (2022); doi: 10.1063/5.0091134
Submitted: 11 March 2022 • Accepted: 23 May 2022 •
Published Online: 11 July 2022

View Online Export Citation CrossMark

S. A. K. Wijethunga,[1,2,a)] M. A. Mamun,[2] R. Suleiman,[2] C. Hernandez-Garcia,[2] B. Bullard,[2] J. R. Delayen,[1,2] J. Grames,[2] G. A. Krafft,[1,2] G. Palacios-Serrano,[2] and M. Poelker[2]

AFFILIATIONS

[1] Old Dominion University, Norfolk, Virginia 23529, USA
[2] Thomas Jefferson National Accelerator Facility, Newport News, Virginia 23606, USA

[a)] Author to whom correspondence should be addressed: sajini@jlab.org

ABSTRACT

The 300 kV DC high voltage photogun at Jefferson Lab was redesigned to deliver electron beams with a much higher bunch charge and improved beam properties. The original design provided only a modest longitudinal electric field (E_z) at the photocathode, which limited the achievable extracted bunch charge. To reach the bunch charge goal of approximately few nC with 75 ps full-width at half-maximum Gaussian laser pulse width, the existing DC high voltage photogun electrodes and anode–cathode gap were modified to increase E_z at the photocathode. In addition, the anode aperture was spatially shifted with respect to the beamline longitudinal axis to minimize the beam deflection introduced by the non-symmetric nature of the inverted insulator photogun design. We present the electrostatic design of the original photogun and the modified photogun and beam dynamics simulations that predict vastly improved performance. We also quantify the impact of the photocathode recess on beam quality, where recess describes the actual location of the photocathode inside the photogun cathode electrode relative to the intended location. A photocathode unintentionally recessed/misplaced by sub-millimeter distance can significantly impact the downstream beam size.

INTRODUCTION

DC high voltage photoguns are used at many accelerator facilities to produce polarized and non-polarized electron beams for a variety of accelerator applications. Jefferson Lab's Continuous Electron Beam Accelerator Facility (CEBAF) uses a DC high voltage photogun to produce highly polarized electron beams at currents ~100 μA and sub-pC bunch charge for nuclear physics research.[1,2] Other applications that employ DC high voltage photoguns include free electron lasers (FELs),[3–6] energy recovery linacs (ERLs),[7,8] and electron cooling;[9,10] these applications typically require very high average current (mA) and high bunch charge (>100 pC).

Most DC high voltage photoguns employ Pierce-geometry focusing electrodes.[11–15] A *Pierce geometry* describes the electrode structure with the surface at a non-zero angle with respect to the vertical direction of the beam axis. This produces a transverse electrostatic force that compensates for the intra-beam Coulomb repulsion force.[16,17] However, the Pierce geometry also reduces the longitudinal electric field E_z at the photocathode, which reduces the maximum extractable bunch charge. Therefore, the ultimate gun design is a trade-off between increasing E_z at the photocathode and adding transverse focusing fields to manage the beam.[18] In our case, since the bunch length is relatively long [~75 ps full-width at half-maximum (FWHM) Gaussian laser pulse width] for high brightness applications, E_z becomes the dominant component to mitigate the space charge effect at nC bunch charge, and thus, flat cathode and anode electrodes are preferred.

Since 2010, Jefferson Lab has pursued an inverted insulator gun design,[11] which has been adopted elsewhere.[19,20] The inverted-insulator design has several advantages, namely, it is compact compared to gun designs that use large cylindrical insulators, which means less surface area, therefore better achievable vacuum. Since the inverted insulator also serves as the electrode support structure, there is less metal biased at high voltage to contribute to field emission. Finally, high voltage is applied to the cathode electrode using a commercial high voltage cable designed to mate with the inverted geometry insulator; thus, there is no exposed high voltage and an SF_6 tank is not required to suppress corona discharge at the photogun.[11,12]

However, the asymmetric photogun design with the inverted insulator geometry creates an asymmetric electric field in the anode–cathode gap. Furthermore, to reliably reach the bias voltage larger than 200 kV, our inverted gun designs include a screening electrode (shield) to minimize the electric field at the insulator–metal–vacuum interface known as the triple point junction.[12] The triple point junction shield is large, which increases the electric field asymmetry, deflecting the beam at the exit of the gun, making it difficult to center in a nearby downstream solenoid, and causing beam losses.

This paper presents the electrostatic design of the modified 300 kV DC high voltage photogun with flat cathode and anode electrodes, resulting in a significantly higher electric field at the photocathode surface. In addition, the new design incorporates a spatially shifted anode, with transverse location adjusted to minimize the unwanted beam deflection caused by the asymmetric inverted insulator design.

Finally, simulations were performed, which quantify the impact of photocathode recess, where recess describes the actual location of the photocathode inside the cathode electrode vs the intended location. In performing the simulations for this work, we learned that the beam is very sensitive to the photocathode position inside the cathode electrode. How much the photocathode is recessed, even by sub-millimeter levels, from the cathode electrode surface can affect the E_z at the photocathode and the beam focusing, and thus, it can impact the size of the beam at viewing screens. Appreciating the importance of knowing the exact location of the photocathode inside the photogun represents an important step toward validating the photogun model and could benefit bright beam applications.

ORIGINAL PHOTOGUN DESIGN

The *Gun design* describes the optimization process whereby electrode and insulator dimensions are varied to reach the desired operating voltage while maintaining desired field strengths and vacuum levels, which implies operation without field emission (which degrades vacuum), or insulator failure due to high voltage breakdown. For our case, the new photogun must operate reliably at 300 kV bias voltage, producing a high-quality beam at nC bunch charge with a 75 ps (FWHM) Gaussian laser pulse width, operating at a 10^{-12} Torr scale vacuum. The vacuum requirement stems from our intention to use this photogun for either unpolarized or polarized electron beam applications, with the polarized beam applications benefiting from the exceptional vacuum.

Vacuum technology has improved dramatically over the years. Standard vacuum practices and commercially available vacuum pumps can provide static 10^{-12} Torr-scale vacuum but only if field emission is kept small/eliminated.[21] Once the electrodes have been polished smooth and cleaned, field emission mainly depends on the maximum electric field strength inside the gun chamber, determined by the applied high voltage, cathode size, radii of curvatures of the components, anode–cathode gap, and the distance to the vacuum chamber walls. Based on our past experience, when the electric field strength inside the gun chamber is <10 MV/m in magnitude, field emission can be negligible following high voltage conditioning.[12]

For inverted gun designs that employ high voltage cables, high voltage breakdown mainly occurs along the high voltage cable termination at the ceramic insulator.[14] The transverse component of the electric field near the triple point junction can drag charged particles toward the insulator surface, inducing a secondary electron emission avalanche, which can then discharge gas that once ionized can lead to this breakdown. In addition, charge accumulation on the insulator surface can lead to breakdown by changing the electric field distribution near the insulator surface. This can be prevented by using a shield that reduces the field strength at the triple point junction. An adequately designed triple point junction shield electrode can also linearize the potential across the insulator.[14] However, since this amplifies the field asymmetry in the anode–cathode gap and the beam deflection at the exit of the anode, the dimensions of the shield should be chosen to minimize both field strength at the triple point junction and beam deflection at the exit of the anode.[22]

To optimize the gun geometry and obtain field maps of the photogun that could be used for particle tracking simulations, the field solver package of *CST Studio Suite*[23] was used. Since the photogun design is cylindrically asymmetric, a 3D modeling software such as *CST Studio Suite* provides more accurate results than 2D electrostatic solver software. Figures 1(a) and 1(b) show the 3D electrostatic model of the original photogun design, with a spherical cathode electrode with a 1.2 cm front face hole and 25° Pierce focusing geometry, and an electrically isolated anode placed 9 cm away from the cathode front. Other relevant features include the inverted ceramic insulator, triple point junction shield, and an array of eight non-evaporable getters (NEG) pump modules. Figure 1(c) shows the electrostatic design on the cathode electrode. The highest fields are found where the radii of curvature are small, but they are almost within the intended range of 0 to −10 MV/m for reliable operation.

Although the original photogun performed well in terms of operating voltage, reaching 360 kV during high voltage conditioning, and operating for months at 300 kV without field emission or breakdown, the problem of the original gun design in terms of high bunch charge delivery is illustrated in Fig. 2. The Pierce electrode geometry provides the desired focusing but unfortunately reduces the electric field at the photocathode surface to less than −3 MV/m, which we have learned is too small to deliver nC charge bunches in our intended 75 ps (FWHM) Gaussian laser pulse width.

As illustrated in Fig. 3, the asymmetric photogun design, enhanced by the large shield electrode needed to prevent high voltage breakdown, and due to the placement of the NEG modules along the body of the photogun vacuum chamber, serves to create a non-uniform electric field within the anode–cathode gap. The figure shows the horizontal and vertical electric field distributions in the anode–cathode gap where the color map (top graphs) shows the E_x and E_y distribution, and the bottom graph shows the magnitude of E_x and E_y along each of the colored dotted lines shown on the field map. Note the small field asymmetry in the x-direction caused by the NEG modules placement, and the large field asymmetry in the y-direction caused by the inverted insulator geometry and shield electrode. The photocathode active area diameter was ~5 mm; hence, the position of each dotted line shown in the top images represents all the possible beam starting locations.

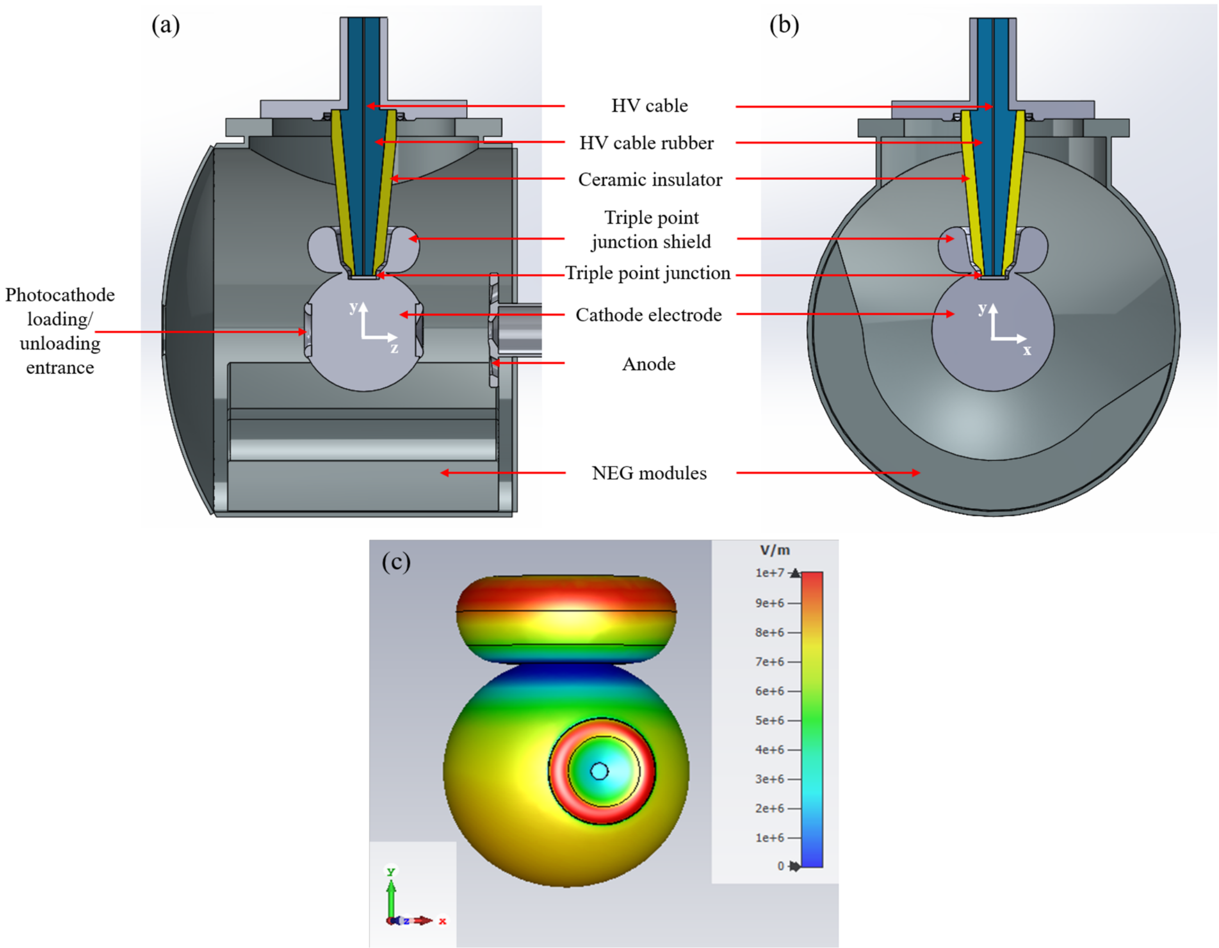

FIG. 1. View cross-sections of the photogun HV vacuum chamber for the original (Pierce) design. (a) Side view with the anode on the right. (b) Front view with the cutting plane in the middle of the spherical electrode, looking from the anode side. (c) Isometric view of the electrostatic simulations showing the gradient on the electrode and its triple junction shield at 350 kV.

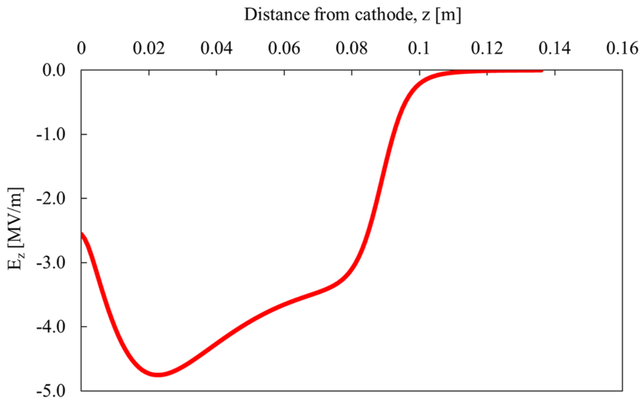

FIG. 2. E_z vs z between the anode–cathode gap when biased at 350 kV for the original (Pierce) design.

To illustrate the impact of asymmetric fields, the particle tracking code General Particle Tracer (GPT)[24] was used to simulate beam transport from the photocathode. Figure 4 shows the beam trajectory in the xz plane (a) and yz plane (b). At 1 m from the gun, the beam deflects ~0.3 cm in the negative x-direction and ~3.3 cm in the negative y-direction. At this location, the diameter of the beampipe is ~6 cm. Steering magnets and focusing solenoids must be employed immediately at the exit of the gun chamber to correct these deflections and minimize beam loss.[25]

E_z at the photocathode sets the limit on the maximum charge density extractable from the photocathode.[26] With E_z ~−1.6 MV/m at the photocathode, we could only deliver 0.7 nC to the dump [225 kV, 75 ps (FWHM) Gaussian laser pulse width, 50 kHz laser repetition rate, and 1.64 mm rms beam size at the cathode].[27] Still, even with these issues, we succeeded in operating this photogun for over 1000 cumulative hours at 300 kV bias voltage with alkali-antimonide photocathodes, which at the time was one of the highest bias voltages ever achieved with an inverted-insulator design.[28]

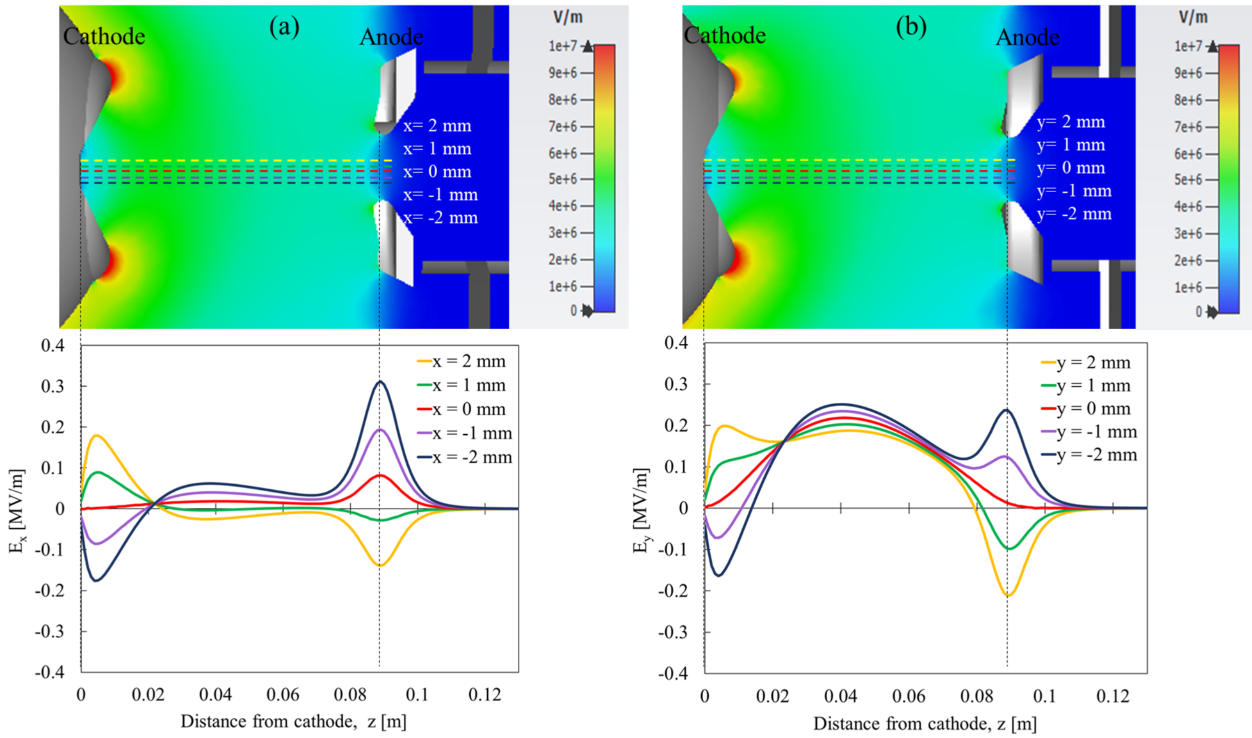

FIG. 3. (a) E_x (looking down) and (b) E_y (looking from side) variations along the dotted colored lines in the anode–cathode gap when the cathode is biased at 350 kV for the original (Pierce) design. Each colored line position represents a possible beam starting point location. The color maps represent the electric field strength in V/m.

MODIFIED ELECTROSTATIC DESIGN

To reach the goal of more bunch charge, the existing DC high voltage photogun was modified to increase E_z at the cathode and to correct the beam deflection exerted by the non-symmetric nature of the inverted insulator photogun, thus making the beam exit the anode centered while minimizing the electric field at triple point junction and field emission.

As described above, E_z at the cathode depends on the bias voltage and the size of anode–cathode gap. Although literature describes the successful operation of DC high voltage photoguns operating at bias voltages >300 kV,[13,15,20] we deemed it prudent to limit operating voltage to 300 kV. Decreasing the anode–cathode gap increases E_z at the cathode, but small gaps create large field strengths, which increases the risk of field emission. Figure 5 shows how E_z varies with the anode–cathode gap ranging from 4 to 9 cm using

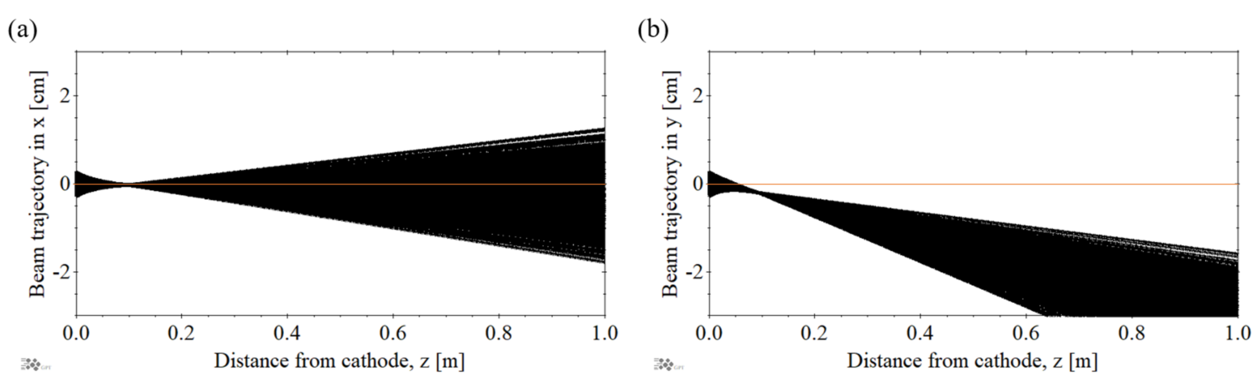

FIG. 4. Beam trajectories: (a) xz plane and (b) yz plane for the original (Pierce) design. [Simulations were performed with 300 kV bias voltage, 1 pC bunch charge, 75 ps (FWHM) Gaussian pulse laser width, 1 mm (rms) laser spot size, no space charge calculations, and no other beamline elements, i.e., no steering or focusing magnets.]

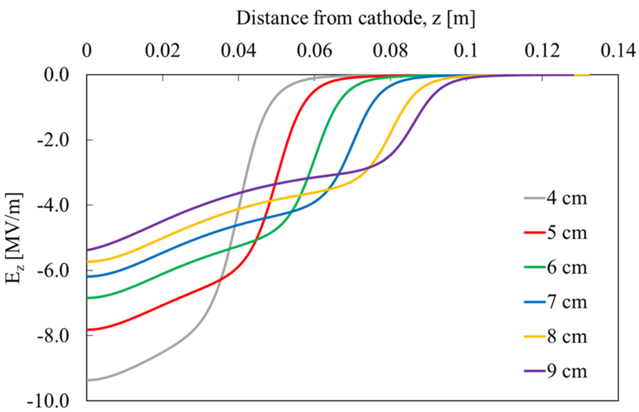

FIG. 5. CST simulations of E_z variation with anode–cathode gap for the modified (flat) design at 350 kV.

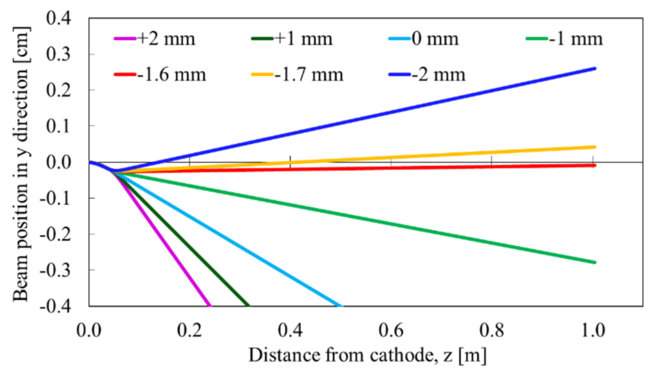

FIG. 7. Closer look of the beam deflection in *y*-deflection for the modified (flat) design.

flat-surface cathode/anode electrodes. The photocathode is located at $z = 0$ m and bias voltage 350 kV (although the intended operation is at 300 kV, voltage headroom is required for conditioning, the gun must survive conditioning at 350 kV, or even higher. Thus, all the simulations were done at 350 kV, conditioning voltage).

Figure 5 shows a considerable increase in E_z at the cathode, compared to the original design, with the flat electrodes providing much of the benefit. For a 9 cm anode–cathode gap, the field strength at 350 kV bias voltage increased from −2.5 to −5.5 MV/m. Reducing the anode–cathode gap provides additional benefits. Although a 4 cm gap gives the highest E_z at the cathode, the maximum field strength in the gun approaches the −10 MV/m limit of concern. Therefore, in order to avoid the field emission risk, we settled on a 5 cm gap with no Pierce geometry, which provides −7.8 MV/m E_z at the cathode, roughly three times the field strength of the original gun design. Note that both electrodes (cathode and anode) were changed to flat to keep the field uniformity in the gap. Also, since the anode was moved from 9 to 5 cm, the locations of the anode holes for the laser beam entering and exiting the gun had to be modified.

According to the simulation, NEG module placement (see Fig. 1) is the main reason for the beam deflection in the *x*-direction. Replacing them with thinner NEG pump modules (or strips) and placing them symmetrically can fix this problem. The deflection in the *y*-direction is mainly due to the inverted insulator geometry and triple point junction shield. After thoroughly examining the design, two simple means were discovered to compensate the effect from the inverted insulator geometry and triple point junction shield, namely, by tilting[29] or displacing the anode electrode. The displaced anode solution is described here.

CST was used to generate field maps for different anode offsets and these field maps were then used in GPT to calculate beam deflections. Figure 6 shows how beam deflection varies with anode shift (a) in *x*- and (b) in *y*-directions, and Fig. 7 illustrates a closer look at how the beam deflects in the *y*-direction for each anode shift. Since the anode was shifted only in the vertical direction, there is no effect on the deflection in the *x*-direction; however, beam position varies significantly in the *y*-direction. For the anode displaced by −1.6 mm, the beam deflection caused by the photogun asymmetric design is nearly countered, and beam travels approximately parallel to the beamline axis, which was our intended goal, minimizing the need to steer beam at the photogun exit. GPT was

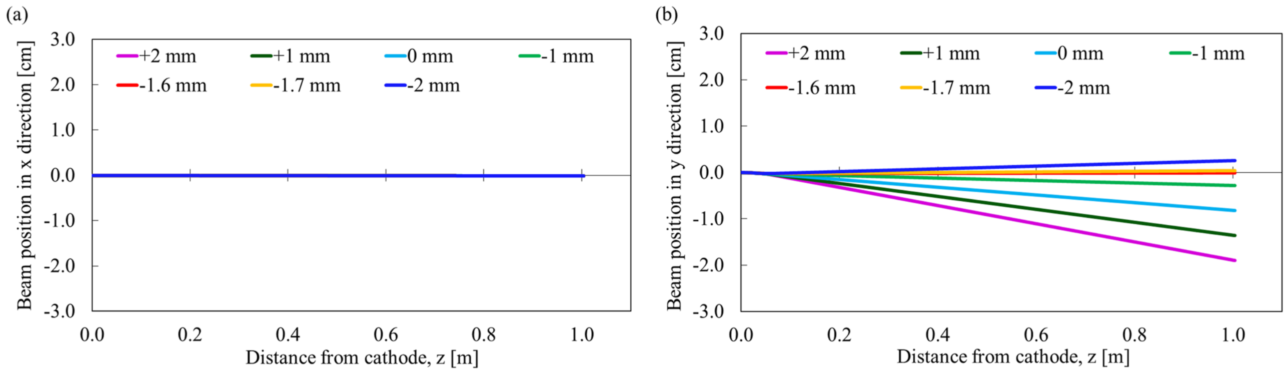

FIG. 6. Beam deflection varies with anode shift. (a) *x*-deflection. (b) *y*-deflection for the modified (flat) design. Since all the anode shifts are in the *y*-direction, there is no effect on the beam position in *x*-direction; thus, all the plots lie on top of each other.

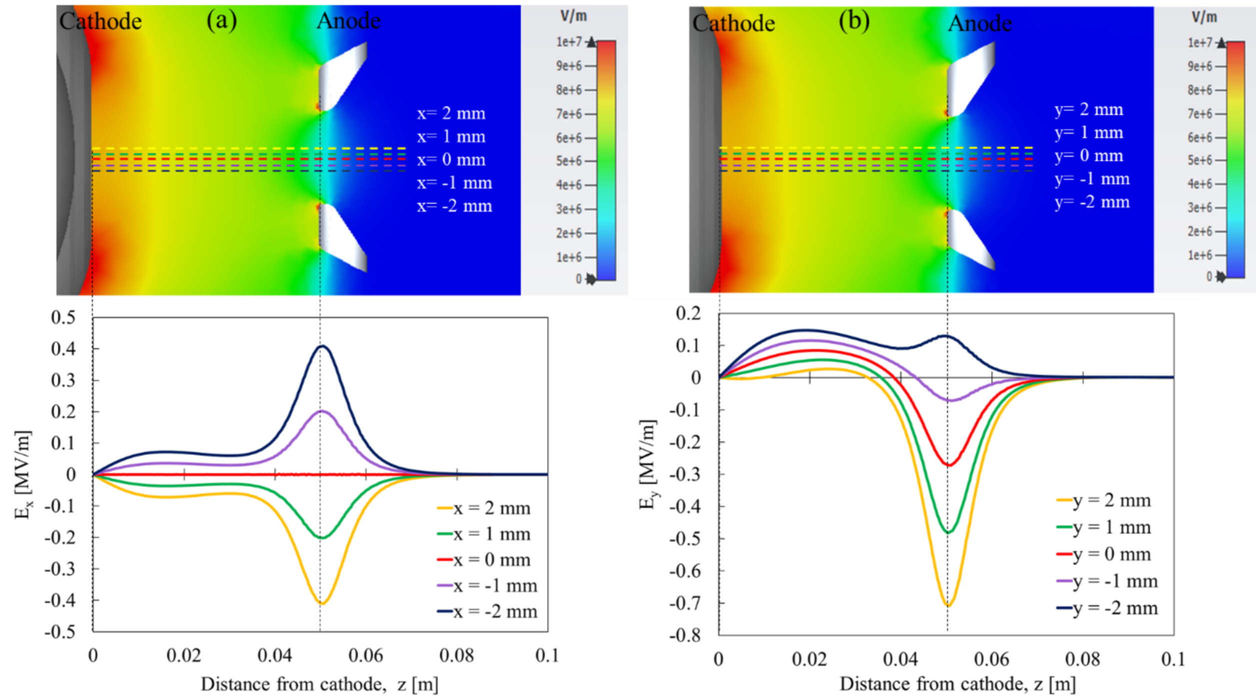

FIG. 8. (a) E_x and (b) E_y variations along the dotted colored lines in the anode–cathode gap for the modified (flat) design with −1.6 mm anode shift when biased at 350 kV. Each colored line position represents a possible beam starting point location. The color maps represent the electric field strength in V/m.

also used to confirm that the −1.6 mm anode offset canceled the deflection of the beam coming out of the center of the photocathode, almost independent of the gun's high voltage.

The horizontal and vertical electric field distributions in the anode–cathode gap for the final design with a −1.6 mm anode shift are illustrated in Fig. 8 where the color maps (top graphs) show the E_x and E_y distributions, and the bottom graphs show the magnitude of E_x and E_y along each of the colored dotted lines shown on the field map.

Figure 9 illustrates how normalized emittance depends on the anode shift in x (a) and y (b). An initial thermal emittance value of 0.64 mm mrad[30] was used in the GPT simulations. In Fig. 9, the rise and fall of the beam emittances in the anode–cathode cap should be ignored; these variations are due to nonlinear radial

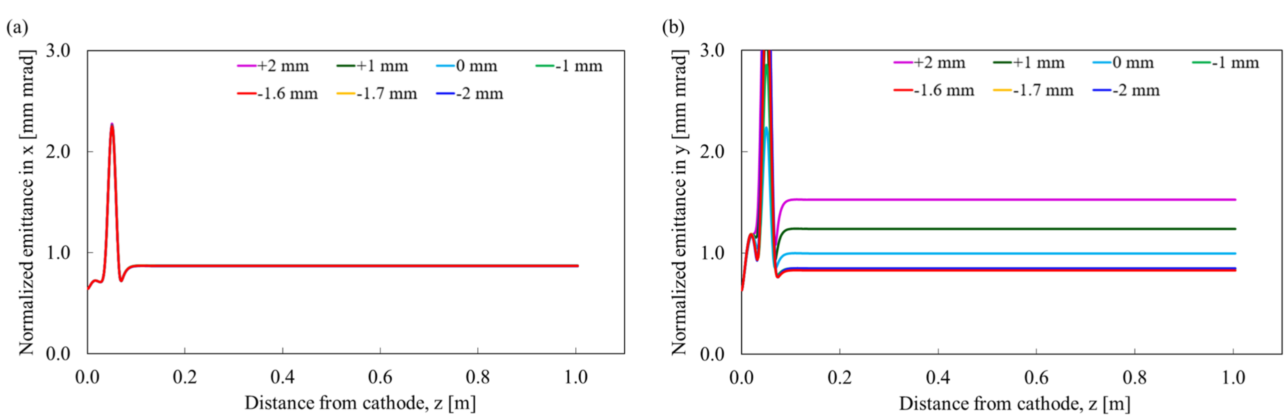

FIG. 9. Normalized emittance variation for the modified (flat) design with the anode shift (a) x and (b) y. Since all the anode shifts are in the y-direction, there is no effect on the normalized emittance in the x-direction; thus, all the plots lie on top of each other.

electric fields, as explained in Refs. 31 and 32. Only the initial and final emittance values downstream are relevant. The increase in emittance coming out of the gun is due to geometrical aberrations.[17] The farther the beam goes off-axis, the larger the curvatures of the E-field, and consequently, the larger the contribution of aberration to beam emittance. For no anode displacement, the emittance in the y-direction is about 1.0 mm mrad. For anode offset of -1.6 mm, emittance still increases but only to 0.83 mm mrad. Aberrations also increase the normalized emittance in the x-direction but since all the anode shifts are in the y-direction, there is no effect on the normalized emittance in the x-direction; thus, all the plots lie on top of each other.

To implement the offset anode, it is not easy to shift the whole anode as it breaks the symmetry of the anode mounting flanges and the laser path. Therefore, after confirming how much shift is needed, a new model was designed with only the anode aperture shifted by -1.6 mm while keeping the anode structure centered and aligned with the cathode and beam pipe. According to the simulations, both give the same results. Each electrode was polished to obtain a mirror-like surface condition using various grades of sandpaper, diamond-paste polishing, and finally barrel polishing.[33] Figure 10 shows both electrodes.

MEASUREMENTS AND SIMULATION RESULTS

The new photogun design was tested with beam to verify that the shifted anode (by -1.6 mm) produced an electron beam centered in the downstream beampipe and with minimal vertical deflection. When operating the old photogun, to the center of the beam on the first viewing screen 1.5 m from the gun, two steering magnets located between the photogun and the viewing screen provided the necessary field integral of 80 G cm to kick the beam vertically upward. Only 20 G cm horizontal was necessary to compensate for the deflection due to the NEGs. For the new design, less than 5 G cm was required in both the vertical and horizontal directions to compensate for the background magnetic fields and any misalignment in the gun and beamline.

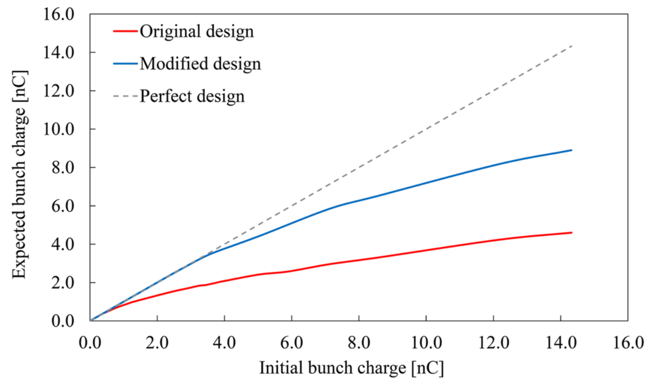

FIG. 11. GPT simulations of expected bunch charge at the cathode vs initial bunch charge from the original (Pierce) design, the modified (flat) design [300 kV, 75 ps (FWHM) Gaussian laser pulse width, 1.2 mm (rms)], and from a perfect design.

Figure 11 shows the GPT simulations of the expected charge from the cathode at 0.5 m for different initial bunch charges for the original and modified photoguns operating at 300 kV. The "initial bunch charge" is the bunch charge that started GPT simulations. The dashed line represents the case of a perfect gun where the extracted charge is equal to the expected charge. Loss-free charge extraction increased significantly using the modified photogun. In order to reduce the beam loss further, the beamline must be modified by removing the components that have small beampipe apertures (e.g., differential pump module). It would also be beneficial to add more Faraday cups along the beamline to track the beam loss.

PHOTOCATHODE RECESS AND BEAM SIZE

While studying the original photogun, we learned the importance of knowing the exact location of the photocathode within the cathode electrode. The measured beam size at viewing screen

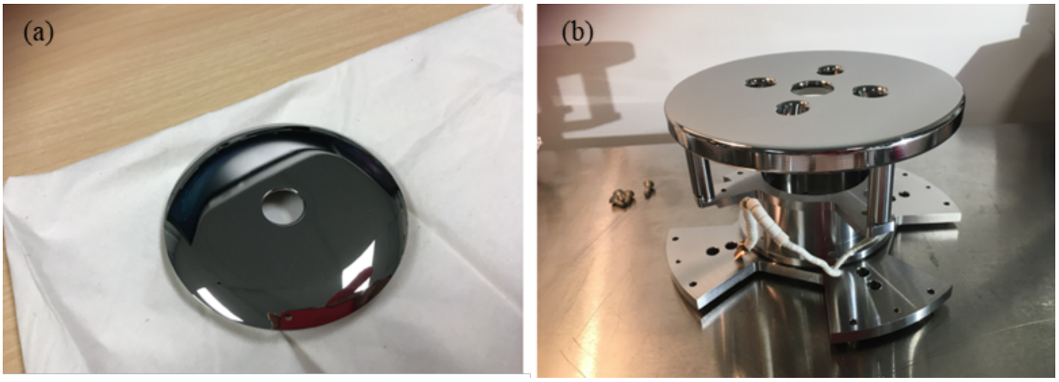

FIG. 10. For the modified (flat) design: (a) front surface of the flat cathode that mates the spherical ball electrode shown in Fig. 1 and (b) the flat anode. The anode aperture (the hole at the center of the anode) is shifted by -1.6 mm. The anode can be biased,[30] with wire visible in the photo. The two of the other four holes are for laser in and out and the other two for viewing the photocathode with a camera.

locations near the photogun was always much larger than predicted by GPT simulations. When the experiment was over, we opened the gun chamber and measured the photocathode position inside the cathode electrode and found that it can be recessed up to 1 mm. CST was used to make field maps of the photogun with different recess values. GPT simulation accurately predicted measured beam size but only by retracting the photocathode surface relative to the photocathode's intended location. Figures 12(a) and 12(c) show the predicted beam size in the x- and y-directions for different photocathode recess locations from 0 mm (no recess) to 1 mm. The black-dot data points in Figs. 12(a) and 12(c) show the measured beam size at the first viewing screen and Figs. 12(b) and 12(d) show a closer look at the beam size inside the anode–cathode gap. As shown in Fig. 12, larger recess lengths increase the focusing strength of the electrode (equivalent to a larger Pierce angle), moving the beam waist closer to the photogun, and resulting in a larger than expected beam at the first viewing screen.

Another problem caused by the photocathode recess is that it reduces the E_z at the photocathode. 1 mm recess reduces E_z at the photocathode from −2.19 to −1.67 MV/m at 300 kV (with Pierce geometry), which will limit the maximum charge density extractable from the photocathode.

In the laboratory, there are plausible explanations for why the photocathode could be recessed inside the cathode electrode. Attaching the photocathode substrate to the puck involves indium solder and a tantalum cup retaining ring that combined with variations in puck dimensions could lead to fit-up variations from photocathode sample to sample. The spring-loaded sapphire rollers designed to push the puck against the interior surface of the cathode electrode may not provide sufficient force. The simulations described here highlight the importance of improved quality control and suggest a redesign of the spring rollers intended to precisely position the photocathode inside the gun.

Similar plots—beam size variation along z for different recess amounts—are shown in Fig. 13 for the new photogun design with flat electrodes. Interestingly, Fig. 13 shows the opposite effect on the beam sizes in terms of photocathode recess. As expected for the ideal condition with no photocathode recess, the flat electrodes provide no focusing and there is no beam waist between the photocathode and the first viewing screen. However, with a recess, the beam is focused, and for large recess amounts, a beam waist is formed in the anode–cathode gap. For a gun with flat electrodes, the recess serves to focus the beam, like a Pierce geometry. For both the old and new gun designs, the recess has a negligible effect on the beam emittance.

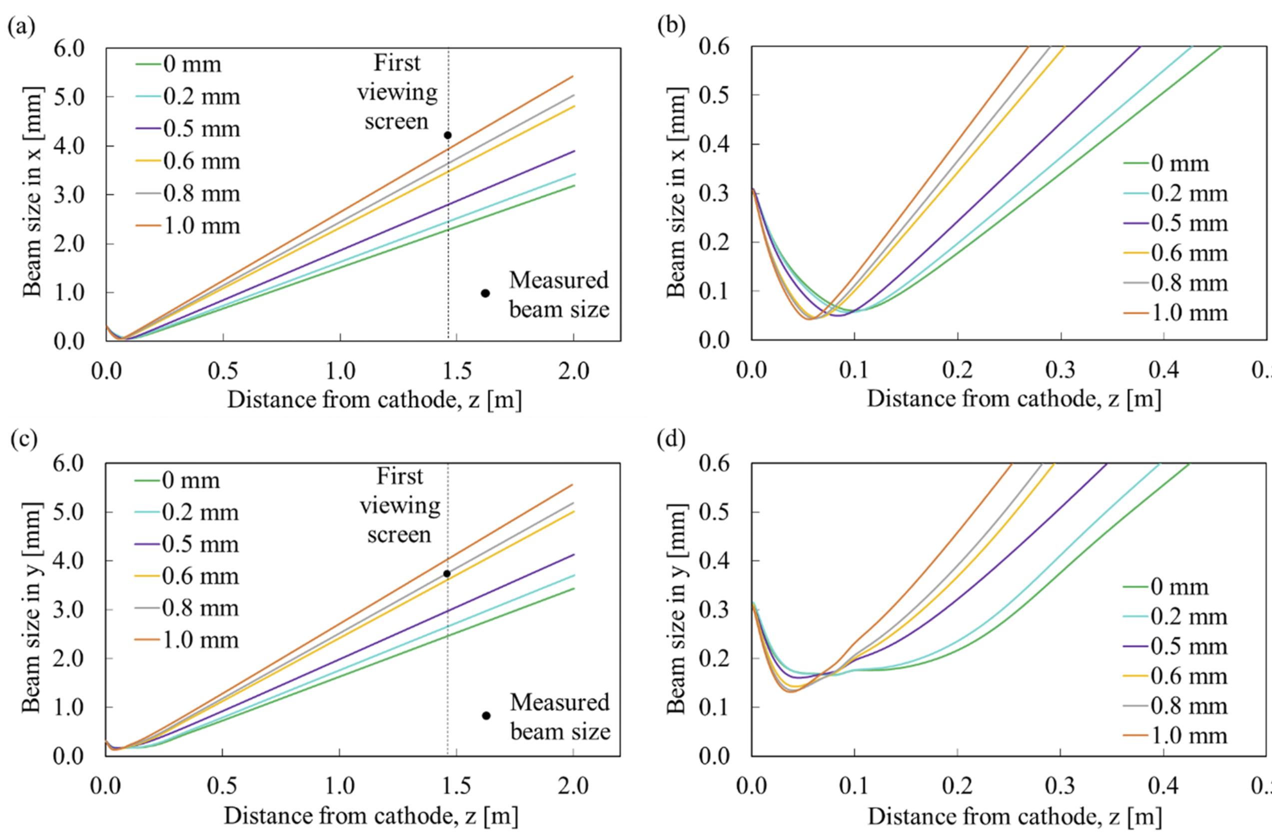

FIG. 12. Simulation showing the variation in beam size in the z-direction for different photocathode recess lengths in the original (Pierce) design. (a) and (c) The beam sizes in x- and y-directions, respectively, with the beam size at the first viewing screen annotated. (b) and (d) Detail over the first 0.5 m of the beamline.

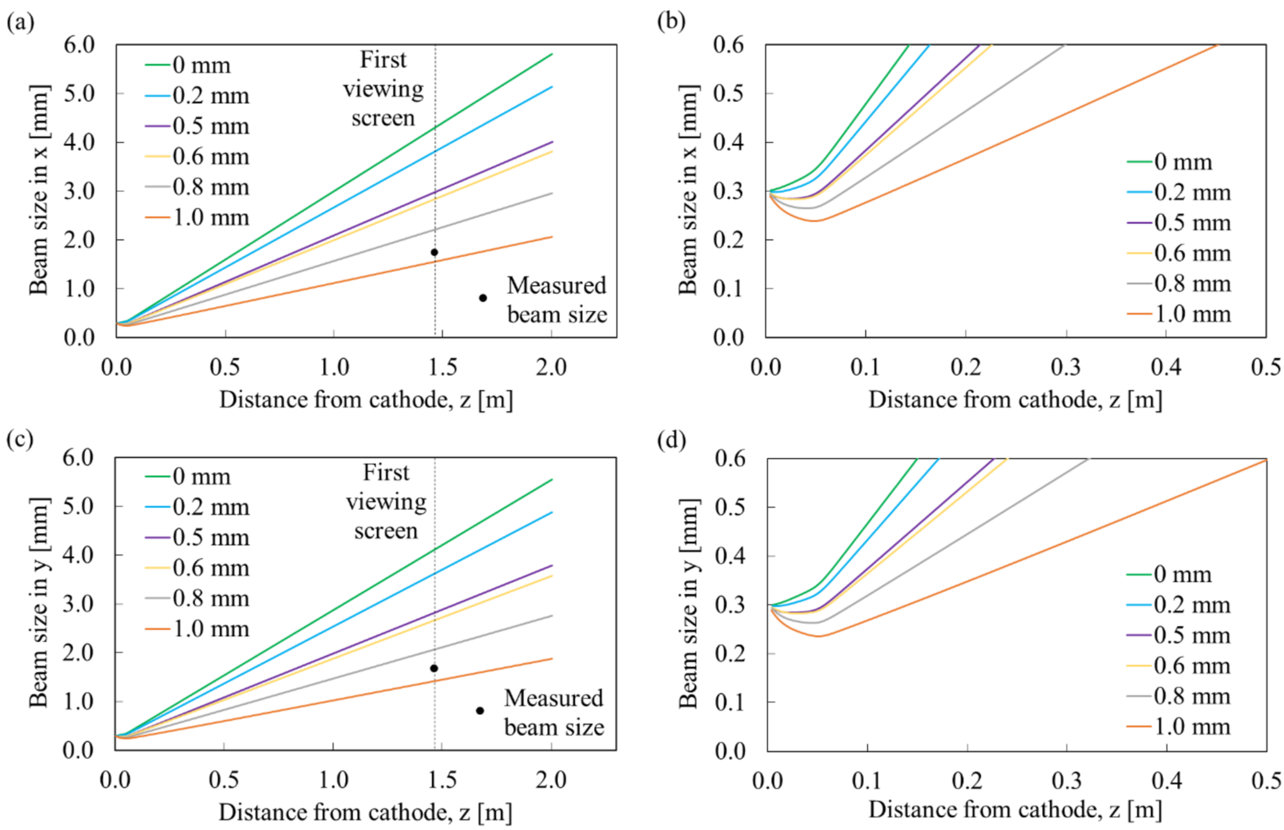

FIG. 13. Simulation showing the variation in beam size in the *z*-direction for different photocathode recess lengths in the modified (flat) design. (a) and (c) The beam sizes in *x*- and *y*-directions, respectively, with the beam size at the first viewing screen annotated. (b) and (d) Detail over the first 0.5 m of the beamline. The photocathode in the modified gun has a similar recess as in the original gun since the interior of the cathode electrode and the photocathode holder (puck) were not modified.

DISCUSSION

Jefferson Lab's 300 kV photogun was re-designed using CST and GPT software to obtain a higher E_z at the photocathode for high bunch charge operations and to correct beam trajectory deflections inherent to the inverted insulator geometry design. The longitudinal electric field magnitude E_z was increased from −2.5 to −7.8 MV/m by removing the Pierce geometry and decreasing the anode–cathode gap from 9 to 5 cm. Our simulation results show that extracted bunch charge from the photocathode should double before accounting for beam loss, as demonstrated in Fig. 11.

It was relatively easy to implement the offset anode but this relatively simple modification provided a significant improvement in photogun performance. A modest downward shift of just 1.6 mm can eliminate beam deflection. All of the photoguns with inverted insulator design will benefit from this modification by reducing beam loss at the anode, thus improving the photocathode lifetime, particularly those at high bunch charge. A tilted anode can be used to accomplish the same goals, and that will be studied in the future.

Finally, while attempting to benchmark simulations with beam size measurements, it became clear the importance of the photocathode position inside the cathode electrode. Experimentally, this can affect E_z at the photocathode and the focusing inside the photogun. Very small displacements of the photocathode from the intended position can have a very big impact on measured beam sizes and a negligible effect on beam emittance. Going forward, the pucks and the interior of the cathode electrode have to be modified to make sure there is no recess. Furthermore, the measured beam size on the first viewing screen will routinely be compared to the simulation to make sure there is no problem with the recess.

ACKNOWLEDGMENTS

This work was supported by the U.S. Department of Energy, Office of Science, Office of Nuclear Physics (Contract No. DE-AC05-06OR23177), the JSA initiatives fund program, and the Laboratory Directed Research and Development program.

AUTHOR DECLARATIONS

Conflict of Interest

The authors have no conflicts to disclose.

Author Contributions

S. A. K. Wijethunga: Conceptualization (equal); Data curation (lead); Formal analysis (lead); Investigation (equal); Methodology (equal); Validation (equal); Visualization (lead); Writing – original draft (lead); Writing – review & editing (equal). **M. A. Mamun:** Conceptualization (equal); Data curation (equal); Investigation (equal); Methodology (equal). **R. Suleiman:** Conceptualization (equal); Data curation (equal); Investigation (equal); Project administration (equal); Resources (equal); Supervision (equal); Writing – review & editing (equal). **C. Hernandez-Garcia:** Conceptualization (equal); Data curation (equal); Formal analysis (equal); Investigation (equal); Methodology (equal); Supervision (supporting); Validation (equal); Writing – review & editing (supporting). **B. Bullard:** Methodology (equal). **J. R. Delayen:** Supervision (supporting); Writing – review & editing (equal). **J. Grames:** Conceptualization (supporting); Project administration (supporting); Supervision (supporting). **G. A. Krafft:** Conceptualization (equal); Supervision (supporting); Writing – review & editing (equal). **G. Palacios-Serrano:** Investigation (supporting); Software (supporting); Writing – review & editing (supporting). **M. Poelker:** Supervision (supporting); Writing – review & editing (lead).

DATA AVAILABILITY

The data that support the findings of this study are available from the corresponding author upon reasonable request.

REFERENCES

[1] C. K. Sinclair, P. A. Adderley, B. M. Dunham, J. C. Hansknecht, P. Hartmann, M. Poelker, J. S. Price, P. M. Rutt, W. J. Schneider, and M. Steigerwald, "Development of a high average current polarized electron source with long cathode operational lifetime," Phys. Rev. Spec. Top.–Accel. Beams **10**, 023501 (2007).

[2] R. Barday and K. Aulenbacher, "Polarized electron source operation at average currents of several milliamperes," AIP Conf. Proc. **915**, 1019 (2007).

[3] G. R. Neil *et al.*, "The JLab high power ERL light source," Nucl. Instrum. Methods Phys. Res., Sect. A **557**, 9 (2006).

[4] S. Benson *et al.*, "High power operation of the JLab IR FEL driver accelerator," in *Proceedings of the 22nd Particle Accelerator Conference, PAC-2007, Albuquerque, NM* (IEEE, New York, 2007).

[5] J. Feldhaus, J. Arthur, and J. B. Hastings, "X-ray free-electron lasers," J. Phys. B: At. Mol. Opt. Phys. **38**, S799 (2005).

[6] C. Hernandez-Garcia, P. G. O'Shea, and M. L. Stutzman, "Electron sources for accelerators," Phys. Today **61**(2), 44–49 (2008).

[7] E. J. Minehara, "Development and operation of the JAERI superconducting energy recovery linacs," Nucl. Instrum. Methods Phys. Res., Sect. A **557**, 16 (2006).

[8] A. Bartnik, N. Banerjee, D. Burke, J. Crittenden, K. Deitrick, J. Dobbins, C. Gulliford, G. H. Hoffstaetter, Y. Li, W. Lou, P. Quigley, D. Sagan, K. Smolenski, J. S. Berg, S. Brooks, R. Hulsart, G. Mahler, F. Meot, R. Michnoff, S. Peggs, T. Roser, D. Trbojevic, N. Tsoupas, and T. Miyajima, "CBETA: First multipass superconducting linear accelerator with energy recovery," Phys. Rev. Lett. **125**, 044803 (2020).

[9] A. V. Fedotov *et al.*, "Experimental demonstration of hadron beam cooling using radio-frequency accelerated electron bunches," Phys. Rev. Lett. **124**, 084801 (2020).

[10] M. A. Al Mamun, P. A. Adderley, J. F. Benesch, B. Bullard, J. R. Delayen, J. M. Grames, J. Guo, F. E. Hannon, J. C. Hansknecht, C. Hernandez-Garcia, R. Kazimi, G. A. Krafft, M. Poelker, R. S. Suleiman, M. G. Tiefenback, Y. Wang, S. Zhang, and S. Wijethunga, "Production of magnetized electron beam from a DC high voltage photogun," in 9th International Particle Accelerator Conference, Vancouver, BC, Canada, 2018.

[11] P. A. Adderley *et al.*, "Load-locked dc high voltage gas photogun with an inverted-geometry ceramic insulator," Phys. Rev. Spec. Top.–Accel. Beams **13**, 010101 (2010).

[12] C. Hernandez-Garcia *et al.*, "Compact −300 kV dc inverted insulator photogun with biased anode and alkali-antimonide photocathode," Phys. Rev. Spec. Top.–Accel. Beams **22**, 113401 (2019).

[13] C. Hernandez-Garcia, M. Poelker, and J. Hansknecht, "High voltage studies of inverted geometry ceramic insulators for a 350 kV DC polarized electron gun," IEEE Trans. Dielectr. Electr. Insul. **23**, 418–427 (2016).

[14] G. Palacios-Serrano *et al.*, "Electrostatic design and conditioning of a triple point junction shield for −200 kV DC high voltage photogun," Rev. Sci. Instrum. **89**, 104703 (2018).

[15] N. Nishimori *et al.*, "Experimental investigation of an optimum configuration for a high-voltage photoemission gun for operations at ≥500 kV," Phys. Rev. Spec. Top.–Accel. Beams **17**, 053401 (2014).

[16] J. R. Pierce, *Theory and Design of Electron Beams*, 2nd ed. (Van Nostrand, New York, 1954).

[17] M. Reiser, *Theory and Design of Charged Particle Beams* (John Wiley & Sons, Inc., 2008), Vol. 7, p. 599.

[18] J. M. Maxson, I. V. Bazarov, K. W. Smolenski, and B. Dunham, "Optimization of DC photogun electrode geometry," in Proceedings of the Particle Accelerator Conference, New York, 2011.

[19] K. Smolenski, I. Bazarov, B. Dunham, H. Li, Y. Li, X. Liu, D. Ouzounov, and C. Sinclair, "Design and performance of the Cornell ERL DC photoemission gun," AIP Conf. Proc. **1149**, 1077–1083 (2009).

[20] W. Liu, O. Rahman, and E. Wang, "High voltage design of a 350 kV DC photogun at BNL," in Proceedings of the North American Particle Accelerator Conference (NAPAC'19), Lansing, MI, 2019.

[21] C. K. Sinclair, High voltage DC photoemission electron guns-current status and technical challenges, ICFA Statement, 2008, https://icfa.usa.jlab.org/archive/newsletter/icfa_bd_nl_47.pdf.

[22] Y. Wang *et al.*, "300 kV DC high voltage photogun with inverted insulator geometry and CsK_2Sb photocathode," in 9th International Particle Accelerator Conference, Vancouver, BC, Canada, 2018.

[23] See http://www.cst.com for CST Studio Suite's.

[24] See http://www.pulsar.nl/2 for General Particle Tracer.

[25] S. A. K. Wijethunga, M. A. Mamun, R. Suleiman, P. Adderley, B. Bullard, J. Benesch, J. R. Delayen, J. Grames, C. Hernandez-Garcia, F. Hannon, R. Kazimi, G. A. Krafft, G. Palacios Serrano, M. Poelker, M. Stefani, Y. Wang, and S. Zhang, "Generation and characterization of magnetized electron beam from DC photogun for electron beam cooling application" (unpublished).

[26] I. V. Bazarov, B. M. Dunham, and C. K. Sinclair, "Maximum achievable beam brightness from photoinjectors," Phys. Rev. Lett. **102**, 104801 (2009).

[27] S. A. K. Wijethunga *et al.*, "Space charge study of the Jefferson Lab magnetized electron beam," in Proceedings of the North American Particle Accelerator Conference (NAPAC'19), Lansing, MI, 2019.

[28] E. Wang, O. Rahman, J. Skaritka, W. Liu, J. Biswas, C. Degen, P. Inacker, R. Lambiase, and M. Paniccia, "High voltage dc gun for high intensity polarized electron source," Phys. Rev. Accel. Beams **25**, 033401 (2022).

[29] S. A. K. Wijethunga, Ph.D. thesis, Old Dominion University, 2021.

[30] Y. Wang *et al.*, "Thermal emittance and lifetime of alkali-antimonide photocathodes grown on GaAs and molybdenum substrates evaluated in a −300 kV dc photogun," Phys. Rev. Accel. Beams **23**, 103401 (2020).

[31] S. B. van der Geer, M. J. de Loos, J. I. M. Botman, O. J. Luiten, and M. J. van der Wiel, "Nonlinear electrostatic emittance compensation in kA, fs electron bunches," Phys. Rev. E **65**, 046501 (2002).
[32] R. Ganter, B. Beutner, S. Binder, H. H. Braun, T. Garvey, C. Gough, C. Hauri, R. Is-chebeck, S. Ivkovic, F. Le Pimpec, K. Li, M. L. Paraliev, M. Pedrozzi, T. Schietinger, B. Steffen, A. Trisorio, and A. Wrulich, "Electron beam characterization of a combined diode rf electron gun," Phys. Rev. Spec. Top.–Accel. Beams **13**, 093502 (2010).
[33] C. Hernandez-Garcia, D. Bullard, F. Hannon, Y. Wang, and M. Poelker, "High voltage performance of a dc photoemission electron gun with centrifugal barrel-polished electrodes," Rev. Sci. Instrum. **88**, 093303 (2017).